

A Polarization Sensitive Bolometric Detector for Observations of the Cosmic Microwave Background

W.C. Jones^a, R.S. Bhatia^a, J.J. Bock^{a,b}, A.E. Lange^a

^aCalifornia Institute of Technology, Pasadena, CA, USA

^bJet Propulsion Laboratory, Pasadena, CA, USA

ABSTRACT

We have developed a bolometric detector that is intrinsically sensitive to linear polarization which is optimized for making measurements of the polarization of the cosmic microwave background radiation. The receiver consists of a pair of co-located silicon nitride micromesh absorbers which couple anisotropically to linearly polarized radiation through a corrugated waveguide structure. This system allows simultaneous background limited measurements of the Stokes I and Q parameters over $\sim 30\%$ bandwidths at frequencies from ~ 60 to 600 GHz. Since both linear polarizations traverse identical optical paths from the sky to the point of detection, the susceptibility to systematic effects is minimized. The amount of uncorrelated noise between the two polarization senses is limited to the quantum limit of thermal and photon shot noise, while drifts in the relative responsivity to orthogonal polarizations are limited to the effect of non-uniformity in the thin film deposition of the leads and the intrinsic thermistor properties. Devices using NTD Ge thermistors have achieved NEPs of $2 \cdot 10^{-17}$ W/ $\sqrt{\text{Hz}}$ with a $1/f$ knee below 100 mHz at a base temperature of 270 mK. Numerical modelling of the structures has been used to optimize the bolometer geometry and coupling to optics. Comparisons of numerical results and experimental data are made. A description of how the quantities measured by the device can be interpreted in terms of the Stokes parameters is presented. The receiver developed for the BOOMERANG and *Planck* HFI focal planes is presented in detail.

Keywords: Sub-mm Detectors, Bolometers, Cosmic Microwave Background Polarization, Cosmology

1. INTRODUCTION

Observational cosmologists have yet to detect polarization in the cosmic microwave background radiation (CMB), and upper limits are still well above the level expected due to Thompson scattering of quadrupole anisotropies in the background radiation during the epoch of recombination.^{1,2} The small amplitude of this polarized signal, peaking at perhaps $5\mu\text{K}$ at $\sim 10'$ scales, demands not only extremely high raw sensitivity, but also exquisite control of systematics.

Over the last twenty years, nearly all published efforts to detect polarization in the CMB have used coherent receivers.* Heterodyne, quasi total-power, and correlation receivers with front-end RF low noise amplifier blocks based on HEMTs are mature technologies at millimeter wavelengths. The fundamental design principles of these receivers are well established and have been used to construct polarized receivers at radio to mm-wave frequencies for many years.^{4,5} Although cryogenic bolometric receivers achieve far higher instantaneous

Corresponding Author:

William Jones, 1200 E. California Blvd., MC 59-33, Pasadena CA 91125. email: wcj@astro.caltech.edu, tel: 626.395.2020

© 2002 Society of Photo-Optical Instrumentation Engineers. This paper will be published in the SPIE *Proceedings* and is made available as an electronic preprint with permission of SPIE. One print or electronic copy may be made for personal use only. Systematic or multiple reproduction, distribution to multiple locations via electronic or other means, duplication of any material in this paper for a fee or for commercial purposes, or modification of the content of the paper are prohibited.

*To the author's knowledge, the pioneering efforts of Caderni, et al., are the only published CMB polarization limits set by a bolometric system.³

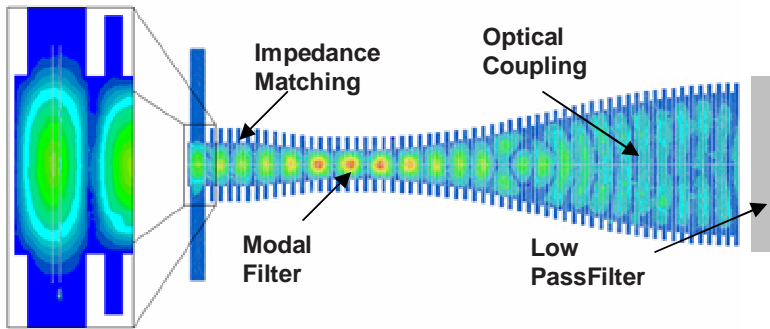


Figure 1. An instantaneous image of the field distribution in BOOMERANG’s corrugated coupling feed. The radiation is incident from the right where low-pass filters and, in some applications, additional optical elements are located. The two bolometers are symmetrically spaced at $\lambda_g/4 + (-) 30\mu\text{m}$ from the backshort in order to maximize coupling efficiency. Similar feed structures have been designed for *Planck*, QUEST and BICEP^{6,7} at 100, 150, 217, and 350 GHz.

sensitivities over wider bandwidths than their coherent analogs, the intrinsic polarization sensitivity of coherent systems has made them the choice of the first generation of CMB polarization experiments.

In this paper we describe a new bolometric system which combines the sensitivity, bandwidth, and stability of a cryogenic bolometer with the intrinsic polarization capability traditionally associated with coherent systems. In addition, the design obviates the need for orthogonal mode transducers (OMTs), hybrid tee networks, waveguide plumbing, or quasi-optical beam splitters whose size and weight make fabrication of large format arrays impractical. Finally, unlike OMTs or other waveguide devices, these systems can be relatively easily scaled to ~ 600 GHz, limited at high frequencies only by the ability to reliably manufacture sufficiently small single-moded corrugated structures. Polarization sensitive bolometers (PSBs) are fabricated using the proven photolithographic techniques used to produce ‘spider web’ bolometers, and enjoy the same benefits of reduced heat capacity, negligible cross section to cosmic rays, and structural rigidity.⁸

Polarization sensitivity is achieved by controlling the vector surface current distribution on the absorber, and thus the efficiency of the ohmic dissipation of incident Poynting flux. This approach requires that the optics, filtering, and coupling structure preserve the sense of polarization of the incident radiation with high fidelity. A multi stage corrugated feed structure and coupling cavity has been designed which achieves polarization sensitivity over a 33% bandwidth. A next generation of sub-orbital, ground based, and orbital bolometric CMB polarization experiments, including BOOMERANG, BICEP, QUEST, and the *Planck* HFI are basing their receiver designs around the PSB concept.

2. GENERAL DESIGN

The PSB design has been driven by the desire to minimize systematic contributions to the polarized signal. Both senses of linearly polarized radiation propagate through a single optical path and filter stack prior to detection, thereby assuring both detectors have identical spectral pass bands and quantum efficiencies. This results in nearly identical background loading and closely matched responsivities between the two detectors. Two orthogonal free standing lossy grids, which are separated by $\sim 60\mu\text{m}$ and both thermally and electrically isolated, are impedance matched to terminate a corrugated waveguide structure. The physical proximity of the two detectors assures that both devices operate in identical RF and thermal environments. A printed circuit board attached to the module accommodates load resistors and RF filtering on the leads entering the cavity. The post detection electronics consist of a highly stable AC readout with a system $1/f$ knee below 100 mHz. Unlike coherent systems, this low frequency stability is attained without phase switching the RF signal.

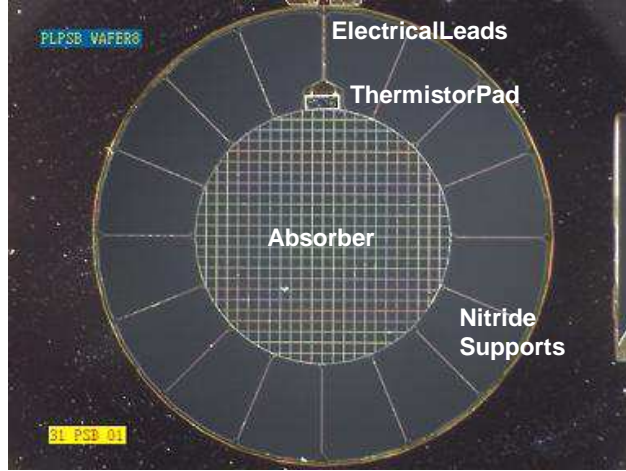


Figure 2. A photograph of a BOOMERANG PSB absorber. The diameter of the grid is 2.6mm, while the absorber leg spacing, g , is $108 \mu\text{m}$. Each leg is $3\mu\text{m}$ wide. This device is sensitive to incident radiation polarized in the vertical direction due to the metallization of the Si_3N_4 mesh in that direction. The horizontal Si_3N_4 beams evident in the photo are un-metallized, and provide structural support for the device. The thermal conductivity between the absorber and the heat sink is dominated by the metallic leads running to the thermistor chip.

2.1. Optics

We have designed the optical elements, including the feed antenna and detector assembly, to preserve sky polarization and minimize instrumental polarization of unpolarized light. To this end, the detector has been designed as an integral part of the optical feed structure.

Corrugated feeds couple radiation from the telescope to the detector assembly. Corrugated horns are the favored feed element for high performance polarized reflector systems due to their superior beam symmetry, large bandwidth, and low sidelobe levels. In addition, cylindrical corrugated feeds and waveguide preserve the orientation of polarized fields with higher fidelity than do their smooth walled counterparts.

The coupling structure, which is cooled to 300 mK, consists of a profiled corrugated horn, a modal filter, and an impedance matching section which allows efficient coupling to the polarization sensitive bolometer (see Figure 1). In addition to a reduction in the physical length of the structure, the profiled horn provides a nearly uniform phase front which couples well to the other filters and optical elements in the system. The modal filter isolates the detectors from any unwanted higher order modes that may be excited in the thermal break. Equivalently, this filter completely separates the design of the bolometer cavity from that of the feed which couples to the optics. The impedance matching section (the re-expansion at the left side of Figure 1) produces a uniform vector field distribution with a well defined guide wavelength[†] and characteristic impedance over a large ($\sim 33\%$) bandwidth.

2.2. Detector assembly

The detector assembly is a corrugated waveguide terminated with impedance-matched loads which have a weak thermal link to the temperature bath. An electric field drives currents through the absorber surfaces which result in ohmic power dissipation. This power is detected as a temperature rise measured by means of matched Neutron Transmutation Doped (NTD) Germanium thermistors.¹⁰ The bolometers each couple to a single (mutually orthogonal) linear polarization by properly matching each absorber geometry to the vector field of the coupling structure. The coupling structure has been tailored to ensure that the field distribution at the location of the bolometer resulting from a polarized source is highly linear. The detector assembly forms

[†]The guide wavelength, λ_g , is typically 20% larger than free space, and $d \log(\lambda_g)/d \log(\nu)$ remains small over the entire range of operation.

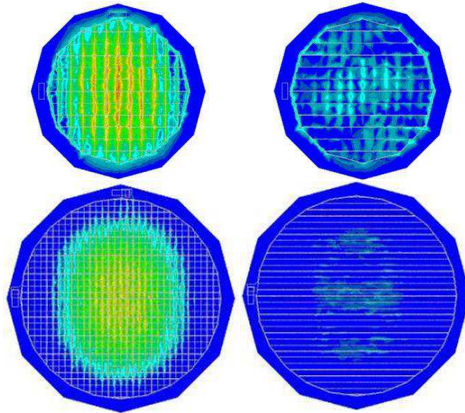


Figure 3. Plots of the Poynting flux through the surface of the bolometer for the prototype PSBs (top) and the 143 GHz PSBs designed for the *Planck* HFI (bottom). For each type of detector, the leftmost plot corresponds to the co-polar device, while the rightmost plot is the cross-polar device. The source polarization is vertical. The intensity and physical scale is the same for all four plots. The superior cross polar performance of the *Planck* device is visually evident in the reduced cross-polar Poynting flux. Integration of the component of the Poynting vector normal to a surface completely inclosing each of the bolometers provides a numerical estimate of the polarization efficiency, $\varpi = 1 - \epsilon$. For the devices shown above the results are shown in Figure 6, and correspond to cross polar leakages, ϵ , of about 5% (prototype) and 1.5% (*Planck*) across the band. Color, animated versions of the above figures, and others, are available from the author upon request.

an RF tight Faraday cage around the bolometers, and both the signal and bias lines are buffered by onboard RF filters.

Because the absorber geometry influences the field distribution within the coupling structure, a treatment of the bolometer cavity as a black body is in general *not* valid. An important consequence of this fact is that any attempt to model an analogous multi-moded optical system will have to carefully consider interference terms between modes when calculating coupling efficiencies or simply trying to predict radiation patterns. The amplitude and phase of any higher order modes capable of propagating to the bolometer depend on the details of both the excitation and structure. Therefore, any numerical calculation would be susceptible to a large number of uncertainties associated with the appropriate boundary conditions at the bolometer, while an accurate analytic solution would be exceedingly difficult. For this reason, it may prove difficult to extend the general single mode PSB design to a multi-moded application without sacrificing cross polar performance.

2.3. Absorber

Each bolometer consists of a linear absorber geometry designed to couple independently to a single linear polarization. PSBs are made using fabrication techniques originally developed for the successful ‘spider-web’ bolometers developed at JPL.^{8,11} They consist of a free standing mesh of low stress Si_3N_4 with a ~ 120 Å thick layer of gold deposited on ~ 20 Å of titanium as a thin film absorber. The thermistor is located at the edge of the absorbing mesh, well into the groove of the corrugations, in order to minimize its effect on the optical coupling and to maximize the thermal efficiency of the device (see Figure 2).

Optimal coupling efficiency requires careful impedance matching of the PSB to the coupling structure. For a given absorber geometry, impedance matching is achieved by controlling the thickness of the absorber metalization and therefore the cold surface impedance of the device. The surface impedance resulting in the highest power coupling efficiency is dependent not only on the geometry of the coupling structure and the frequency of operation, but also on the geometry of the absorber.

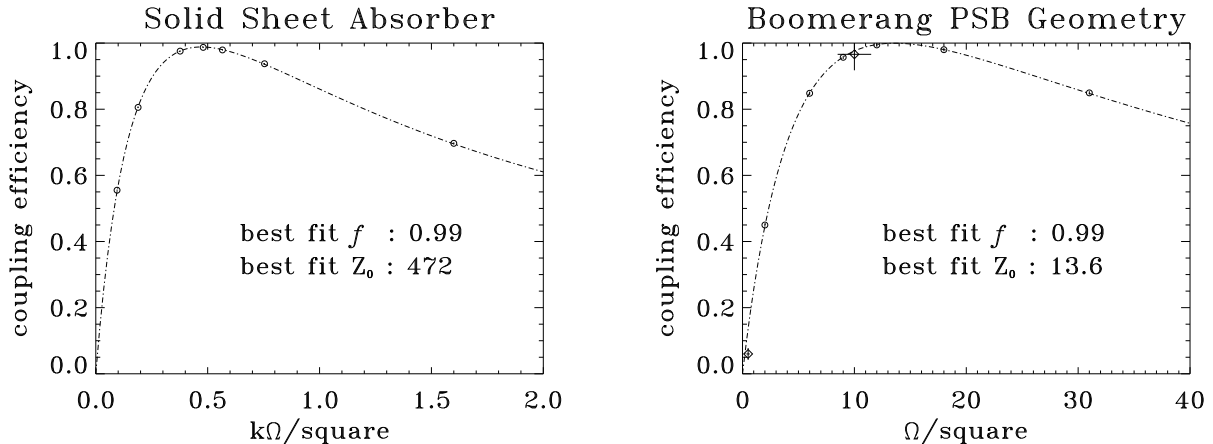


Figure 4. At left, the numerically determined coupling efficiency, $\eta(Z_{\text{abs}})$, of a solid sheet of uniform surface impedance mounted in a PSB coupling structure. The open circles are the numerical results. A function of the form of Equation 1 is fit to the points to determine the peak coupling efficiency and characteristic impedance of the structure at the center frequency of the operational band. At right, the same numerical procedure is performed for the particular geometry of the BOOMERANG PSBs. Note the change in scale of the abscissa, from $k\Omega$ to Ω , which can be understood in terms of the filling factor of the PSB absorber (see Equation 2). For the BOOMERANG geometry, two absorber metallizations were fabricated and tested, corresponding to approximately $0.5 \Omega/\text{square}$ and $10 \Omega/\text{square}$. The measured coupling efficiency of the two types of devices are indicated by the open diamonds, and are in excellent agreement with the numerical result. The error bars represent the uncertainty in the cold impedance of the metallization layer and the transmission of the window material and optical filters.

This fact can be understood in terms of classical transmission line theory. For an idealized transmission line of characteristic impedance Z_0 terminated in a load with impedance Z_{load} one expects a reflection amplitude (S_{11} , normalized to input) of

$$|S_{11}| = \left| \frac{Z_0 - Z_{\text{load}}}{Z_0 + Z_{\text{load}}} \right|$$

In the limit that the characteristic spacing of the absorber grid is much less than a wavelength, the transmission line model is applicable to the PSB coupling. In order to parameterize the power coupling efficiency as a function of bolometer surface impedance, we use the functional form suggested by transmission line theory,

$$\eta(Z_{\text{abs}}) = f \times \left[1 - \left(\frac{Z_0 - Z_{\text{abs}}}{Z_0 + Z_{\text{abs}}} \right)^2 \right] \quad (1)$$

where f and Z_0 are free parameters, while Z_{abs} is determined by the processing of the absorber.

In order to determine the optimal absorber impedance for our devices, numerical computations of $\eta(Z_{\text{abs}})$ were made for discrete values of Z_{abs} using the Ansoft HFSS package.¹² These results were used to determine f and Z_0 for each of six device geometries at the center frequency of our band. The geometries included a solid sheet, a “spider-web” bolometer, and four types of PSBs, all of which were found to be well fit by the functional form of Equation 1. The results of the numerical procedure for two of the devices, a solid sheet and the PSB design chosen for BOOMERANG, are shown at the left and right of Figure 4, respectively. The best fit surface impedances ranged from $470 \Omega/\text{square}$ for the solid sheet to nearly $5 \Omega/\text{square}$ for the device with the finest absorber leg widths.

In order to validate both the numerical procedure and the application of transmission line theory to the PSB coupling, optical efficiency measurements of devices with physical surface impedances of $\sim 0.5 \Omega/\text{square}$ and

$\sim 10 \Omega/\text{square}$ were made. The numerical, theoretical, and measured efficiencies are compared in Figure 4 at right. The well matched devices showed optical efficiencies nearly a factor of four higher than the low impedance devices, and validate the applicability of transmission line theory to the PSB coupling structure.

Similar numerical simulations were made of a smooth walled conical feed exiting into an integrating cavity. This structure was found to deviate significantly from the transmission line theory and showed little dependence on the details of the absorber geometry, presumably because the abrupt discontinuity in the boundary conditions at the entrance to the cavity dominate the return loss.

The results of the numerical computations suggest that it is not possible, in principal, to analytically calculate the optimal absorber surface impedance for an arbitrary geometry due to the fact that the characteristic impedance of the structure, Z_0 , is itself dependent on the web geometry. However, in the limit that the absorber geometry approaches a solid resistive sheet, the characteristic impedance of the PSB coupling structure approaches $Z_0 \rightarrow 470 \text{ Ohms}$. This numerically determined characteristic impedance is greater than that of free space (377 Ohms), as is to be expected for an electrically small structure.

An approximate relationship for the optimal target surface impedance of a given absorber geometry can then be obtained in the following way. Imagine making N infinitesimally thin slices through a solid sheet absorber of this surface impedance. Clearly Z_0 , the optimal surface impedance of a solid sheet, is still the appropriate target impedance. If one then reduces the width, w , of each of the $N + 1$ legs of the absorber without adjusting the physical surface impedance from Z_0 , the *optically* active area will no longer have the same characteristic impedance. For a given absorber diameter D and center to center leg spacing $g = \frac{D}{N+1}$, each leg will be acting for an optical area which is fixed ($g \times L$), while its geometric area ($w \times L$) is clearly not. Therefore, one would expect that the optimal target surface impedance would scale as the ratio of geometric area to optical area,

$$Z_{\text{abs}} \approx Z_0 \frac{w}{g} = Z_0 \frac{w(N+1)}{D} \quad (2)$$

so that in the limit that the filling factor approaches unity the surface impedance, Z_{abs} , approaches Z_0 . For g 's less than $\lambda/5$, we have found good agreement between this approximate relation and numerical calculations of the optimal surface impedance of a given absorber geometry. For reference, the BOOMERANG devices have 23 absorber legs of width $w \simeq 3\mu\text{m}$, and a 2.6 mm absorber diameter (see Table 1). Using the Z_0 determined from a solid sheet absorber, application of Equation 2 yields an optimal impedance of $12.5 \Omega/\text{square}$, versus the numerically determined value of 13.6.

2.4. Thermal Design

The bolometer design must ensure that the power deposited on the absorber is efficiently detected by the thermistor. The parasitic thermal conductivity of the Si_3N_4 supports and inefficient heat transport across the absorber can potentially result in a loss of detector efficiency if a significant fraction of the optical power dissipated in the absorber does not result in a temperature rise of the thermistor. For this reason, several features were built into the PSB design to ensure sufficient thermal efficiency.

The electrical leads constitute the dominant thermal path from the bolometer to the temperature bath. The thermistor is located on a pad which is heat sunk to both the leads and the absorber via a thermally conductive ring surrounding the absorber. For the extremely low background bolometers with thermal conductivities below 30 pW/K , the Si_3N_4 beam supporting the leads has been found to be a significant contribution to the total thermal conductivity. The scaling of the thermal conductance with temperature for these devices is consistent with a T^3 dependence, as described in Holmes, et al.¹³

A finite element thermal model of the bolometer design was implemented in order to analyze the thermal efficiency of the bolometer design. The thermal conductance and heat capacity of the metallization and Si_3N_4 structures used by the model were obtained empirically in independent analysis of similar structures.^{13,14} The thermal model allows the calculation of the temperature rise at the thermistor resulting from power (DC and AC) dissipated on the absorber, the bolometer response to a transient pulse of power deposited on the absorber (similar to a cosmic ray hit), and the ratio of power flow through the thermistor to the total power deposited on the bolometer.

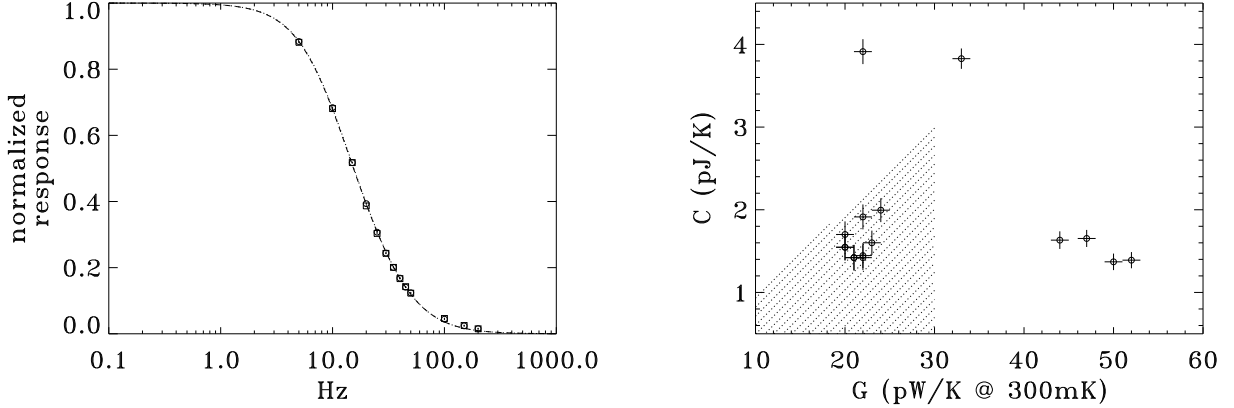


Figure 5. The thermal properties of the prototype PSBs. At left, the measured response of a PSB pair to a chopped optical source. The two devices, which are over-plotted, are very well matched in τ and therefore well matched in both heat capacity and thermal conductivity. At right, a plot of the measured heat capacity versus thermal conductivity for a variety of PSB devices at 300mK. The cross-hatched region is the region of parameter space acceptable for BOOMERANG’s 150 GHz PSBs.

The response of the device to a chopped source was measured over a ~ 1 kHz bandwidth. The measured bolometer response agrees very well with the finite element model. The calculated ratio of rise time to relaxation time for a transient pulse is $\sim 10\%$ at 400 mK, which indicates that the crossing time for temperature fluctuations across the absorber is much less than the thermal time constant of the bolometer. Finally, the results of the thermal analysis indicate that the ratio of power flow through the thermistor to the total power deposited on the mesh is 0.97 for the prototype devices.

3. POLARIZED SIGNAL ANALYSIS

The two bolometers in a PSB pair can be read out either in a bridge circuit or individually. A bridge circuit has the advantage of measuring the difference signal directly through a single amplifier chain, however it requires close matching of the thermistor properties and does not provide a precise simultaneous measurement of I . For the study of the cosmic background radiation, it is highly advantageous to measure both the polarized and unpolarized components simultaneously.¹⁵ In the remainder of this paper we will consider the signals received by the bolometers individually. An analysis of the individual readout illustrates the fundamental properties of the PSBs and how they can be interpreted in terms of the Stokes parameters.

3.1. PSB readout

In a suitably defined coordinate system the measured signal voltage is

$$v_i = S_i \cdot \frac{1}{2} \int d\nu \lambda^2 \eta_i F_i(\nu) [(1 + \epsilon_i) \cdot I \pm (1 - \epsilon_i) \cdot (Q \cos(2\alpha_i) + U \sin(2\alpha_i))] \quad (3)$$

where the sign of the polarized term is associated with the copolar (+) or crosspolar (−) device, S_i is the voltage responsivity of the bolometer, λ^2 is the throughput ($A\Omega$) of the system, and the product $\eta_i F_i(\nu)$ is the absolute spectral transmission. The crosspolar leakage, ϵ_i , is the quantity measured in Figure 6, and can be thought of as the response of a device to a 100% linearly polarized source oriented perpendicular to the design axis of sensitivity. Equivalently, one could define a polarization efficiency of the detector, $\xi \equiv 1 - \epsilon$, which, as is shown below, enters as a multiplicative factor in the overall efficiency of the system to polarized radiation. The

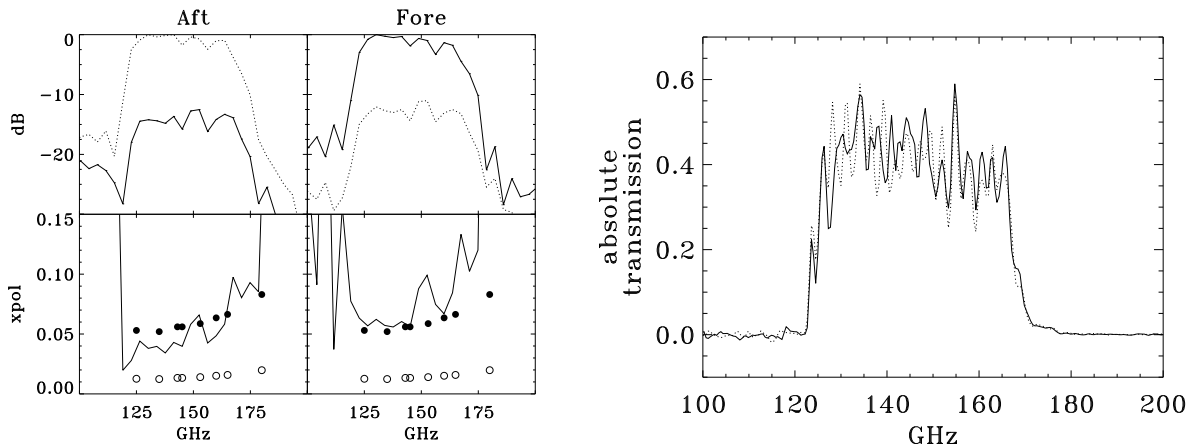


Figure 6. At left, the measured cross-polar performance of a prototype (Type 04) PSB in the BOOMERANG testbed. The upper panels show the measured spectra in the two orthogonal directions defined by the PSB pair. Below, the measured cross-polar leakage, ϵ_i , as a function of frequency for a PSB pair. The spectral resolution of the measurement is 4 GHz and the signal to noise is only significant within the passband, from 124 to 168 GHz. The filled circles indicate the single frequency results of the HFSS simulations. The open circles are the simulation results for the device geometry designed for *Planck*. At right, the measured optical efficiency of the BOOMERANG PSBs. The spectra are taken with a Fourier transform spectrometer at 500 MHz resolution. The spectral normalization is obtained by measuring the electrical power difference at constant resistance with 77K, 90K, 273K, and 300K beam filling loads. The spectra for the two bolometers in a PSB pair are shown, one with a solid line, the other a dotted line.

alignment angle, α_i , is the orientation of the bolometer in the coordinate system which defines Q and U .[‡] The bolometer voltage responsivities, S_i , are dependent on the background power, the temperature of the bath, the thermal conductance, the spectral bandpass, the optical efficiency, and the thermistor properties.

Ideally, the two bolometers would have $\epsilon = 0$ and would be oriented exactly 90° with respect to one another, however in practice the two devices exhibit crosspolar response at the few percent level and are typically orthogonal to within 1.5° . It is important to note that a single PSB cannot fully characterize the polarization of the signal without some method of rotating Q into U , or vice versa. Ideally one would modulate the polarized component of the radiation, as with a wave-plate or Faraday rotator, in order to unambiguously measure both the Stokes Q and U parameters from a single feed. In practice, instruments such as BOOMERANG and *Planck* will rely on scanning through several orientations on the sky in order to build up information on both Q and U .

In a suitably defined coordinate system, $\alpha_1 \simeq 0^\circ$ and $\alpha_2 \simeq 90^\circ$. Therefore, so long as $\epsilon_i \ll 1$, a measurement of I is obtained by summing the two signals while a measurement of Q is obtained by taking the difference. For simplicity, we approximate Equation 3 by removing I, Q , and U from the frequency integral and introduce the factor $\mathcal{F}_i \equiv \int d\nu \lambda^2 \eta_i F_i(\nu)$. Taking the signal difference yields,

$$(v_1 - v_2) = \gamma \cdot I + \delta \cdot Q \quad (4)$$

where we have made the definitions,

$$\gamma \equiv [S_1 \cdot \mathcal{F}_1 \cdot (1 + \epsilon_1) - S_2 \cdot \mathcal{F}_2 \cdot (1 + \epsilon_2)] \quad (5)$$

$$\delta \equiv [S_1 \cdot \mathcal{F}_1 \cdot (1 - \epsilon_1) + S_2 \cdot \mathcal{F}_2 \cdot (1 - \epsilon_2)] \quad (6)$$

The parameter ϵ is identical to a degradation in sensitivity to polarization. The common mode rejection ratio (CMRR) of the PSB receiver depends crucially on the stability of the coefficient γ in Equation 5. For studies

[‡]Kaplan and Delabrouille have investigated the impact of uncertainty in these parameters via Monte Carlo estimation. For reference, it is relatively easy to measure both ϵ and α to a few percent precision, which roughly correspond to the highest precision considered in that analysis.^{16, 17}

of the CMB, the dominant unpolarized signal, I , will be that of the temperature anisotropy. For the currently favored Λ CDM cosmology, the ratio of the polarized to unpolarized power is expected to range from 2-6% over the angular scales of interest, which determines the level of stability required of the parameter γ .[§]

3.2. Polarization efficiency

From Equation 5, it is evident that the stability of γ depends on the stability of both the cross polar leakage and the calibration. The intrinsic polarization efficiency of a PSB is a property of the geometry of the absorber and coupling structure, the metallization of the absorber, and the spectral bandpass.[¶] The numerical simulations provide some intuition about the origin of this cross polar response. For a single frequency, one can integrate the component of the Poynting vector normal to two separate surfaces, each of which fully enclose one of the bolometers. The model used includes the detailed geometry of the absorber, the thermistor, the electrical leads, and all support structures. For a given source polarization, a comparison of the total integrated flux through these surfaces yields the ratio of power absorbed on each bolometer. The results of this numerical procedure for five PSB absorber geometries are presented in Table 1. In all cases, the surface impedance which provided the maximum polarization efficiency was found to coincide with value yielding the peak power absorption. A deviation from optimal surface impedance of $\sim 20\%$ was found to result in a degradation of the polarization leakage by $\sim 12\%$.

Measurements of the cross polarization are in good agreement with the numerically determined values. Two methods were used to measure the cross polar response of the system. A polarized Fourier Transform Spectrometer was used to study the spectral dependence of the polarization efficiency. The left panel of Figure 6 shows the measured spectrum of the cross polar response for a prototype PSB installed in the BOOMERANG testbed at 4 GHz resolution. The filled circles represent single frequency results from numerically integrating the Poynting flux. A second test used a chopped thermal (Rayleigh-Jeans) source and polarizing grid to measure the broadband response as a function of grid orientation. The latter measurement will generally result in a lower polarization efficiency than will result in a measurement of the CMB due to the relatively flat spectrum of the cosmological signal and the rising spectrum of the polarization leakage.

As is evident from Figure 3, a significant fraction of the cross polar response of the prototype devices originates from power dissipation at the edge of the mesh. Another factor found to influence the cross polar response is the line spacing, g . The calculated cross polar level generally declines with a more densely packed grid. In order to determine the effect, if any, of the Si_3N_4 mechanical supports running perpendicular to the absorbing legs on the cross polarization, the support legs of a prototype device were removed by laser ablation after optical testing. Retesting the device showed no change in the level of polarization leakage. The polarization leakage, ϵ , is a material property of the device and is entirely stable.

Finally, an additional effect which can be important is the role of electrical crosstalk between readout channels. Electrical shielding of the bias and signal lines is required to minimize this effect, especially between the two devices within a pair. This crosstalk is indistinguishable from cross polar leakage, ϵ , and must be both carefully avoided and characterized.

3.3. Relative calibration

We have shown that the stability of the relative calibration of the two polarization senses is critical in order to achieve an acceptably small systematic contribution to the signal. This situation is by no means unique to a PSB receiver. Coherent receivers are susceptible to large gain fluctuations and phase error in the front end amplifiers which are analogous, though typically far larger in amplitude, to fluctuations in the product $S_i \cdot \mathcal{F}_i$. For this reason most correlation receivers used in measurements of the CMB use some sort of synchronous demodulation

[§]Specifically, $\langle EE \rangle / \langle TT \rangle$, the ratio of gradient mode polarization to temperature anisotropy bandpowers over angular scales of $\sim 2^\circ$ to $10'$, or $\ell \simeq 400 - 2000$.

[¶]Of course, the efficiency of a given instrument depends as well on the properties of optical arrangement, including the filters, feed elements, reflectors, and window material, etc. At the percent level, we have observed a degradation of polarization efficiency with increased thickness of the window material.

Table 1. Bolometer design parameters for the four prototype device geometries (Types 01– 04), and the *Planck* 143P geometry (type 05). The values of Z_0 and ϵ quoted in the last two columns represent the numerically determined values at 150 GHz. [§] The polarization leakage, defined by Equation 3 is calculated at optimal absorber impedance. [†] The devices geometries used in BOOMERANG. [‡] The device designed for *Planck* HFI’s 143P channels.

PSB Geometry	mesh diameter d [mm]	line width w [μm]	line spacing g [μm]	char. imped. Z_0 [Ω/square]	xpol. leakage [§] ϵ [%]
Type 01 [†]	2.6	3	108	13.6	2.6
Type 02 [†]	2.6	5	108	22.5	2.3
Type 03	2.6	3	325	4.9	5.6
Type 04	2.6	3	217	6.8	5.4
Type 05 [‡]	3.2	3	100	15.4	1.3

of the signal at frequencies above that of the gain fluctuations. As we will see, the PSB architecture is designed to realize stability in the relative calibration at frequencies as low as a few tens of milliHertz.

Fluctuations in the relative calibration arise from mismatched effective throughput, \mathcal{F}_i , as well as drifts in the voltage responsivity, S_i . The right panel of Figure 6 shows band averaged optical efficiencies, essentially $d\mathcal{F}_i/d\nu$, of the BOOMERANG PSBs. The efficiencies are matched to within a few percent, while the band edges are matched to better than 0.2%. The edge of the band is determined by the waveguide cutoff of the feed, while the upper edge is defined by metal mesh resonant filters.¹⁸ Due to the fact that the optical path for each polarization sense is identical, the voltage responsivity will dominate variations in the calibration. As we will see, the great advantage of the PSB architecture is the fact that the factors which determine the relative responsivity are intrinsic to the physical arrangement, and are therefore extremely stable.

Any number of authors have discussed the properties of bolometric receivers; the authoritative treatment is given in the series of papers by Mather.^{19, 20} It can be shown that the voltage responsivity of a bolometer under a given optical load is completely determined by five quantities, the spectral bandpass, the quantum efficiency, the temperature of the bath, the thermal conductance to the bath, and the properties of the thermistor material. We have discussed the first two items, and have shown them to be well matched and extremely stable. The physical proximity of the devices, separated by $< 60\mu\text{m}$ on a beryllium copper housing, ensures that the two devices operate from a common bath temperature. The thermal conductance to the bath is determined by the uniformity of the metal deposition of the electrical leads, and is matched to within $\sim 10\%$ for the devices fabricated on a single wafer for the BOOMERANG PSBs. Better matching is possible for devices with higher thermal conductivity than those designed for BOOMERANG, $G \simeq 20$ pW/K at 300 mK. The final contribution to the difference in responsivity of devices within a PSB pair is the variation in the thermistor properties between the two devices. The NTD germanium thermistors used in this work have a resistance versus temperature well described by

$$R(T) = R_0 e^{\sqrt{\frac{\Delta}{T}}}$$

Variation in the parameter Δ , which is a property of the doping of the germanium, is found to be much smaller than the variation in R_0 , which is dependent on the geometry of the chip. However, both parameters are intrinsic to the chip, and likewise are entirely stable.

4. THE PROTOTYPE RECEIVER

The experimental results reported in this work are primarily the results of the development program for the new BOOMERANG focal plane. The BOOMERANG receiver is a prototype of the *Planck* HFI 143 GHz polarized receiver. We include for completeness the details of this system, so that the data may be interpreted in the proper context.

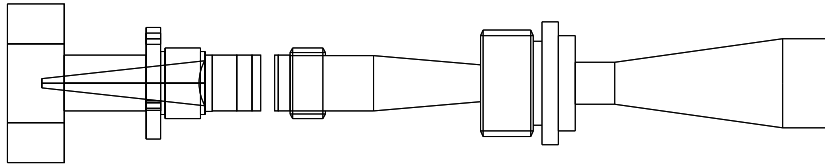


Figure 7. The BOOMERANG 150 GHz PSB feed assembly. The 2K feed, though not a necessary component of the PSB design, is a convenient method of including additional filtering and control of the beam without loss of performance. Both the 2K and sub-K feeds are fully corrugated and profiled to provide high fidelity transmission of the polarized signal, symmetric E and H plane beams, and relatively high gain in a compact system.

In addition to the feed element described in Section 2.1, the prototype optical system consists of a profiled, corrugated back to back feed which is cooled to 2K. This feed defines the lower edge of the operational band, and couples to the reflector system. The high pass edge of the sub-K assembly is designed to be $\sim 10\%$ below that of the 2K feed in order to assure that both the throughput and beam definition are provided by the 2K feed element. Two different 2K feeds were designed and tested, each of which is corrugated in both the front and back sections. Neither of these feeds were found to contribute to the cross polarization or to degrade the optical efficiency when properly configured. However, replacing the sub-K feed with a smooth-walled but otherwise identical feed resulted in a two-fold increase (roughly 5%, absolute) in the crosspolar response, ϵ , of a PSB receiver tested in the BOOMERANG focal plane.

The system has achieved high end-to-end efficiency. A band average efficiency of nearly 40% is measured by calculating the power difference observed between beam-filling loads which are controlled at temperatures of 273 and 300K, as well as 77K and 90K. The right panel of Figure 6 shows the normalized transmission of the system as measured in the BOOMERANG system. This efficiency is not corrected for any loss in the vacuum window material, the blocking filters at 80K and 2K, or the sub-K or 2K feeds.

5. CONCLUSION

We have demonstrated a 300 mK bolometric receiver which is intrinsically sensitive to linear polarization over a 33% bandwidth. The general design is scalable from $\sim 60 - 600$ GHz. This design benefits from reduced susceptibility to systematic effects due to the common filtering, matched beams on the sky, matched time constants, stable relative responsivities, and matched end-to-end efficiencies of each sense of linear polarization. Unlike coherent correlation polarimeters, this receiver simultaneously measures the polarized and unpolarized components of the signal with comparable sensitivity. The design minimizes the size and weight of the receiver, making it especially appropriate for orbital and sub-orbital compact feedhorn arrays. A general method of reliably calculating the optimal absorber impedance for a bolometric detector is presented. The measured performance of the system is in good agreement with the results of the numerical modelling.

ACKNOWLEDGMENTS

The authors would like to acknowledge Peter Ade and Carole Tucker, who kindly provided the optical filters for the development program. Tom Montroy and Ted Kisner provided invaluable information about the performance of the PSBs installed in the BOOMERANG focal plane, and Eric Torbet has measured the polarized spectra of the PSBs integrated in the BOOMERANG focal plane. WCJ would like to thank Kathy Deniston for facilitating this development effort, Goutam Chattopadhyay for his useful comments on the use of the HFSS software package, and Jonas Zmuidzinas, Marcus Runyan, and Brian Jones for helpful discussions. Thanks to Paolo deBernardis for making the authors aware of the early work of Caderni, et al. RSB is currently with the European Space Agency, ESTEC, Noordwijk, The Netherlands. William Jones is supported through NASA GSRP fellowship NGT5-50278. We are grateful for the generous support of this effort by The Caltech Discovery Fund.

REFERENCES

1. S.T. Staggs, J.O. Gundersen, S.E. Church, "CMB Polarization Experiments", astro-ph/9904062, 1999.
2. C. O'Dell, "A New Upper limit on the Polarization of the Cosmic Microwave Background Radiation", astro-ph/0201224, 2002.
3. N. Caderni et al., *Phys. Rev. D.*, **17**, 1908, (1978)
4. T. Gaier, these Proceedings.
5. D. Spiga, et. al. "CMB Observations: improvements of the performance of correlation radiometers by signal modulation and synchronous detection", astro-ph/0202292, 2002.
6. Ki Won Yoon, private communication.
7. B. Keating, these *Proceedings*
8. Minhee Yun, these *Proceedings*.
9. J. Bock, these *Proceedings*.
10. J. Beeman, <http://www.haller-beeman.com>
11. J.J Bock, D. Chen, P.D. Mauskopf, and A.E. Lange, "A novel bolometer for infrared and millimeter-wave astrophysics," *Space Sci. Rev.* **74**, pp. 229-235, 1995.
12. Ansoft High Frequency Structure Simulator, <http://www.ansoft.com>
13. W. Holmes, J.M. Gildemeister, and P.L. Richards, "Measurements of thermal transport in low stress silicon nitride films," *Applied Physics Letters*, **72**, No. 18, 1998.
14. P.D. Mauskopf, J.J. Bock, H. Del Castillo, W.L. Holzapfel, and A.E. Lange, "Composite infrared bolometers with Si₃N₄ micromesh absorbers," *Applied Optics*, **36**, No. 4, 1997.
15. A. de Oliveira-Costa, et. al. astro-ph/0204021, 2002.
16. J. Delabrouille, J. Kaplan, "Measuring CMB polarization with the *Planck* HFI", astro-ph/0112458, 2001.
17. J. Kaplan, J. Delabrouille, "Some sources of systematic errors on CMB polarized measurements with bolometers", astro-ph/0112488, 2001.
18. C. Lee, P.A.R. Ade, and C.V. Haynes, "Self Supporting Filters for Compact Focal Plane Designs", ESA SP-388, pp. 81, 1996.
19. J.C. Mather, "Bolometer noise: nonequilibrium theory", *Applied Optics*, **21**, No. 6, 1982.
20. J.C. Mather, "Bolometers: ultimate sensitivity, optimization, and amplifier coupling", *Applied Optics*, **23**, No. 4, 1984.